

Absolute Configuration of a Cyclic Dipeptide Reflected in Vibrational Optical Activity: Ab Initio and Experimental Investigation

Xiaojun Li,[†] Kathrin H. Hopmann,[⊗] Jana Hudcová,[‡] Wenche Stensen,[§] Jana Novotná,^{||} Marie Urbanová,[⊥] John-Sigurd Svendsen,[⊗] Petr Bouř,^{*,‡} and Kenneth Ruud^{*,†}

[†]Centre for Theoretical and Computational Chemistry (CTCC), Department of Chemistry, University of Tromsø, N-9037 Tromsø, Norway

[‡]Institute of Organic Chemistry and Biochemistry, Academy of Sciences, 166 10 Prague, Czech Republic

[§]Lytix Biopharma AS, Tromsø Research Park, N-9294 Tromsø, Norway

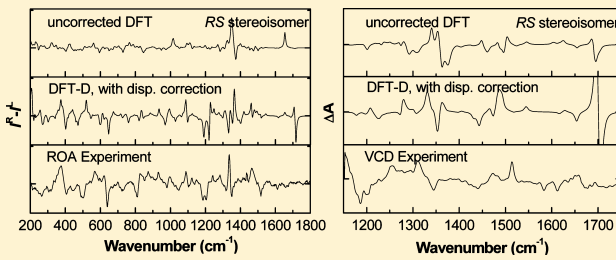
^{||}Department of Analytical Chemistry, Institute of Chemical Technology, Prague, 166 28 Prague, Czech Republic

[⊥]Department of Physics and Measurements, Institute of Chemical Technology, Prague, 166 28 Prague, Czech Republic

[⊗]Department of Chemistry, University of Tromsø, N-9037 Tromsø, Norway

S Supporting Information

ABSTRACT: The ability of Raman optical activity (ROA) and vibrational circular dichroism (VCD) experiments to determine the absolute configuration of chiral molecules with multiple stereogenic centers was explored for four diastereoisomers of a conformationally flexible cyclic dipeptide, cyclo(Arg-Tyr(OMe)). The reliability of the interpretation depended on the correct description of the molecular conformation, which was found to be strongly affected by intramolecular interactions. In particular, when dispersion corrections were included in the density functional theory calculations, the simulated spectra matched the experimental observations well. Experimental and theoretical ROA and VCD spectra were well correlated for all the absolute configurations (RS, SR, SS, and RR) of protonated cyclo(Arg-Tyr(OMe)). These spectroscopies thus appear useful not only for reliable determination of the absolute configuration and conformation but also in revealing the role of hydrogen bonds and C–H···π interactions in the structure stabilization, which can potentially be used when designing enzyme inhibitors and supramolecular architectures.



INTRODUCTION

Cyclic dipeptides, also known as 2,5-diketopiperazines (DKPs), have attracted considerable interest recently.¹ The characteristic heterocyclic ring system of the DKPs can be identified in a variety of biologically active natural products.¹ DKPs are also byproducts of beverage and food processing² as well as being intermediates in protein hydrolysis and in oligopeptide formation.^{3–6} Among the biological activities reported for DKPs are alteration of the cardiovascular and blood clotting systems,⁷ and binding affinity to a variety of receptors including opioid,⁸ GABAoid,⁹ 5-HT1A¹⁰ and oxytocin,¹¹ and calcium channels.⁸ In addition, DPK derivatives may have antitumor,¹² antibacterial,^{13,14} antifungal,¹² and antiviral¹⁵ effects. They have also been used in protein folding studies.^{16,17} The chirality of the cyclic dipeptides determines the supramolecular structures of these compounds and their abilities to engage in molecular recognition arising from their self-assembled hydrogen-bonded structures.^{18,19}

DKPs are the smallest cyclic peptides possible and represent an excellent polypeptide mimic with controlled substituent stereochemistry. Furthermore, the DKP ring contains both hydrogen bonding donor and acceptor moieties and is more

conformationally rigid than linear dipeptides. The cyclic nature of the DKP system also makes it more resistant toward enzymatic proteolysis. DKPs are thus considered ideal privileged structures for the rational discovery and design of new drugs.²⁰

Although density functional theory (DFT) has been widely employed in chemistry and material and biological sciences, most implementations fail to provide a proper description of London dispersion forces.^{21–23} Higher-level correlated quantum chemistry methods (e.g., MP2 or CCSD(T)) are better at describing the many-body forces that govern dispersion interactions. However, their computational cost is usually too high to allow applications of these methods to large molecules of biological interest. Instead, in order to obtain an improved description of dispersion interactions employing DFT, Grimme^{24,25} proposed an empirical $-f(R)C_6/R^6$ correction to DFT functionals. Such an approach is usually referred to as DFT-D. It provides a better description of weak interactions

Received: November 28, 2011

Revised: February 12, 2012

Published: February 15, 2012

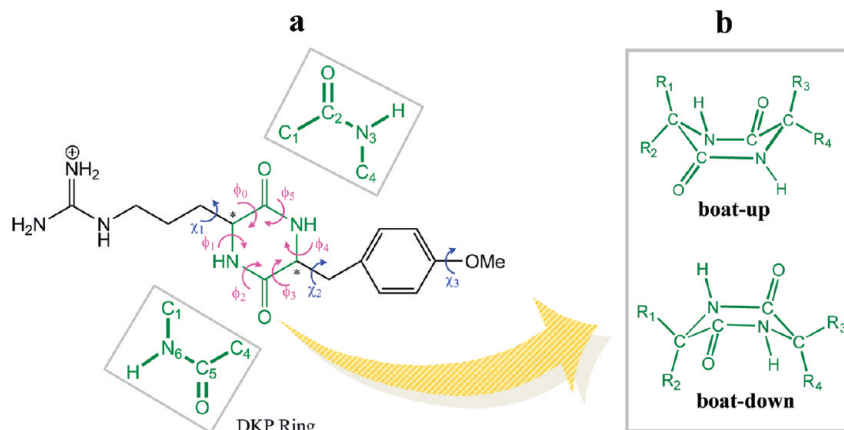


Figure 1. Structure of protonated CATM and (a) the definition of main torsion angles and the atom labeling of the DKP ring; (b) two possible conformations of the DKP ring are boat-up and boat-down forms, in which R_1 and R_2 represent the hydrogen or arginine side chain, while R_3 and R_4 represent the hydrogen or tyrosine(OMe) side chain, respectively.

than uncorrected DFT and has a significantly lower computational cost than correlated wave function calculations.^{26–29}

Vibrational optical activity, including Raman optical activity (ROA)^{30–34} and vibrational circular dichroism (VCD),^{35,36} are chiroptical spectroscopic techniques especially sensitive to molecular conformations and structural variations. They exploit differential scattering (ROA) or absorption (VCD) of right- and left-circularly polarized incident light by chiral molecules. Both techniques have been successfully applied to determine the structure and absolute configuration (AC) of a wide range of molecules ranging from small isolated molecules^{37–39} to oligopeptides,^{40–42} proteins,^{43–45} viruses,^{44,46} and drugs.^{47,48} The vibrational spectra contain many bands sensitive to particular structural features. ROA and VCD are established techniques for determining the AC of molecules with multiple stereocenters;^{48–51} however, these methods have rarely studied all stereoisomers of a compound, and sometimes the VCD technique also fails to resolve all stereocenters.⁵² One of the main goals of this work is to test the reliability of ROA and VCD to discriminate the AC of all stereoisomers both experimentally and theoretically, using a well-defined set of diastereoisomers of a model cyclic dipeptide.

Spectroscopic methods have been applied to cyclic dipeptides extensively, such as IR and Raman,^{53–58} NMR,^{59–62} CD,^{62–65} and UV photoelectron spectroscopy.^{65–67} Although these techniques provide valuable information about molecular and electronic structure, they usually cannot discriminate between diastereoisomers. In the present study, the configurational and conformational analysis of protonated cyclo(Arg-Tyr(OMe)) (CATM, Figure 1) was based on the polarized ROA and VCD spectroscopies. The two chiral centers (marked with asterisks in Figure 1) give rise to four stereoisomers: RS, SR, SS, and RR, where, e.g., RS = 1R,4S. CATM plays an important role in the antinociceptive activity,⁶⁸ and the side chains have a function in the proposed inhibition mechanism.^{69,70} The compound is small enough to allow for accurate computations, but its bulky and polar side chain can interfere with the AC determination.

The compound was also chosen in view of our previous problems in assigning the configuration of all stereocenters of two marine compounds (Synoxazolidinone A and C),⁷¹ which are similar in size and conformational flexibility to CATM. CATM is a simpler system that can be studied more exhaustively by quantum chemical calculations; in particular, it allows us to

see whether ROA and VCD can discriminate between all individual stereoisomers and to single out the role of dispersion forces and conformations. Our results suggest that DFT-D (but not mere DFT) is able to provide sufficiently accurate data for relative conformer populations and puckering of the six-membered ring and that this is essential for the interpretation of the experimental spectra.

MATERIALS AND METHODS

Experiments. The protonated CATM samples were synthesized at the University of Tromsø following standard procedures. The Raman and ROA spectra were measured at the Institute of Organic Chemistry and Biochemistry (Prague) with the Biotools μ -ChiralRAMAN-2X instrument at room temperature, equipped with an Opus diode-pumped solid-state laser operating at 532 nm. This spectrometer employs backscattering geometry and SCP setup as designed by W. Hug.⁷² The samples were dissolved in deionized water to a concentration of 0.2 M and filled into a quartz microcell with an optical path of 3 mm and a volume of $\sim 40 \mu\text{L}$. The output laser power was 300 mW, (130 mW at the sample). Fluorescence coming from impurities was quenched by leaving the sample in the laser beam for a few hours before the measurement. Total acquisition time was about 21 h for each sample. Solvent signal was subtracted from the Raman spectra, and minor baseline corrections were made. The ROA spectra of RS and SR as well as SS and RR CATM provide nearly opposite ROA sign patterns. Occasional deviations can be explained by noise and instrumental artifacts. The baseline was corrected, and ROA spectra are presented as the differential ROA spectra of two appropriate diastereoisomers.

The IR and VCD spectra were measured at the Institute of Chemical Technology (Prague) with an IFS66/S FTIR spectrometer equipped with PMA 37 VCD/IRRAS VCD module (Bruker, Germany) using 4 cm^{-1} resolution. Each spectrum was accumulated for 3–7 h. The samples were dissolved in CD_3OD to a concentration of 0.1 M. The solutions were placed in CaF_2 cells with a $50 \mu\text{m}$ path length. The spectra were corrected for a baseline obtained as the solvent spectrum measured at the same conditions.

Conformational Search and Optimizations. The protonated CATM structure has four stereoisomers: RS, SR, SS, and RR. For every isomer, $3^5 \times 4 \times 3 = 2916$ conformers were generated using the MCM program⁷³ by varying five

torsion angles on the side chain (120° increments), OMe position (up, down, in plane left, or in plane right), and three conformations of the DKP ring (planar, boat, or chair). However, the number of conformers could be reduced based on a cyclo(Ala-Ala) potential energy surface (PES) and selected main torsion angles. Two cyclo(Ala-Ala) torsion angles defined in Figure S1 of the Supporting Information were constrained between -50 and 50° in 10° increments, which resulted in 121 geometries. These were minimized by energy minimization while relaxing all other coordinates. This analysis indicated that only two DKP ring conformations (boat-up and boat-down, Figure S1, Supporting Information) are possible. Likewise, three torsion angles (χ_{1-3} , Figure 1) on the side chain are regarded as the main torsion angles of the derivatives in which the χ_1 and χ_2 involving the α carbon were varied as -60 , 60 , and 180° ; χ_3 is only determined from two OMe positions (in plane left and in plane right), while the remaining atomic coordinates are allowed to fully relax. In summary, a total of $3^2 \times 2 \times 2 \times 4 = 144$ structures in four stereoisomers were left for structural optimization.

For the six-membered DKP ring, we used the ring-puckering coordinates (Q , θ , and P_2) derived from the endocyclic torsion angles, proposed by Haasnoot with the truncated Fourier (TF) formalism⁷⁴ based on an earlier report by Cremer and Pople (CP).⁷⁵ The endocyclic torsion angles (ϕ_j , $j = 0, 1, \dots, 5$, defined in Figure 1a) in the six-membered ring can be described by the truncated Fourier series:

$$\Phi_j = \Phi_2 \cos(P_2 + 4\pi j/6) + \Phi_3 \cos(\pi j) \quad (1)$$

where the puckering parameters (Φ_2 , P_2 , and Φ_3) may be replaced by a spherical polar set (Q , θ , and P_2) as⁷⁴

$$Q = \sqrt{\Phi_2^2 + \Phi_3^2} \quad (2)$$

and

$$\theta = \arctan(\Phi_2/\Phi_3) \quad (3)$$

where the Q term is the total puckering amplitude with $0 \leq \theta \leq \pi$.

The hybrid B3LYP functional^{76,77} with dispersion corrections^{24,25} (B3LYP-D) and the 6-31++G** basis set as implemented in the Gaussian program⁷⁸ were used to fully optimize the selected structures. We used the IEFPCM model^{79–81} for describing the solvent effects since it can properly treat solvation energies of charged species.⁸² The puckering of the DKP ring was analyzed with respect to the phase and amplitude of the pseudorotation.⁷⁴ For all PES minima, harmonic vibrational frequency calculations were carried out to verify that the optimized geometries correspond to equilibrium structures and not to transition states.

IR, VCD, Raman, and ROA Spectra Generation. On the basis of the B3LYP-D/6-31++G**/IEFPCM(H₂O) optimized structures, IR, VCD, Raman, and ROA intensities were computed using the Gaussian09 (B.01) software package at the same level of theory as the optimization. For VCD, the acidic hydrogens (NH, NH₂) were replaced by deuteria in order to match the experimental environment of CD₃OD. An excitation frequency of 532 nm was used to generate the back-scattered Raman and ROA dynamic polarizabilities. All spectral profiles were produced by a convolution with a Lorentzian function and Boltzmann temperature correction,^{83,84} with the full width at half-maximum of 10 cm⁻¹ at 298 K. For every diastereoisomer, conformer subspectra were averaged using

Boltzmann statistics (298 K) with corrections for the zero-point vibrational energy (ZPVE).

RESULTS AND DISCUSSION

Influence of Dispersion Correction. To illustrate the importance of the involvement of the dispersion forces in the calculation, we compare optimized b1 structures (see Figure 2

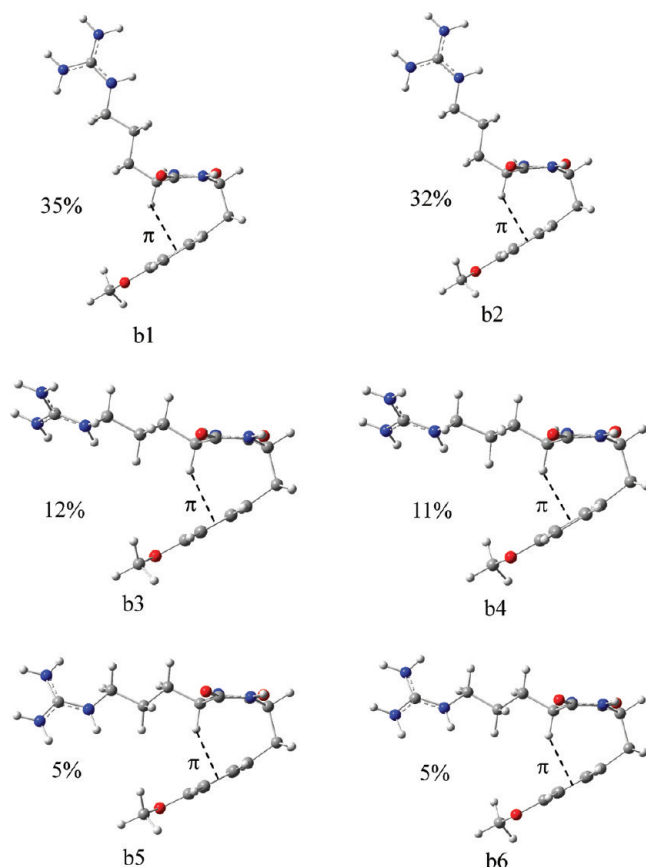


Figure 2. Optimized structures of the six most stable conformers of protonated RS-CATM, obtained at the B3LYP-D/6-31++G**/IEFPCM(H₂O) level of theory. Boltzmann weights calculated from their relative energies with ZPVE correction (see Table 1) are indicated. Note that all conformers are stabilized by the C–H…π (phenyl) interaction.

and Figure S2 of the Supporting Information), as obtained by the B3LYP, B3LYP-D, and MP2 methods (6-31++G**/IEFPCM(H₂O)). As can be seen in Figure S2 (Supporting Information), the B3LYP-D geometry is in good agreement with the reference MP2 geometry, but the pure B3LYP method provides a different structure even for the same conformer due to the lack of dispersion.

Calculated relative conformer energies for the RS isomer are listed in Table S1 (Supporting Information) for 21 conformers. When no dispersion corrections are added, there are many low-energy conformations in which the DKP ring exists in the boat-up, boat-down, and planar forms. With the dispersion correction included, only six conformers are significantly populated at the experimental temperature. These conformations constitute a set of three pairs (e.g., b1 vs b2) with two OMe positions (in plane left and in plane right, see Figure 2), and the DKP ring favors the boat-down conformation. A closer look reveals that these conformers are stabilized by a C_α–H…π

Table 1. Relative Energies (ΔE , kcal/mol), Boltzmann Weights (BW, 298.15 K), $C_{\alpha}-H\cdots\pi$ Distance^a ($d_{C-H\cdots\pi}$ Å), and Pseudorotational Parameters (Q , θ , and P_2 , deg) of Stable RS Conformers with Dispersion Correction for Protonated CATM, Obtained at B3LYP-D/6-31++G***/IEFPCM(H₂O) Level of Theory

conformer	ΔE	ΔE_0^b	BW ^c	$d_{C-H\cdots\pi}$	pseudorotational parameters			
					Q	θ	P_2	shape
b1	0.04	0.00	0.35	2.465	31.67	84.42	229.88	T
b2	0.00	0.04	0.32	2.434	32.44	84.84	229.29	T
b3	0.60	0.65	0.12	2.384	33.57	87.75	228.70	T
b4	0.62	0.69	0.11	2.364	33.80	88.55	227.75	T
b5	0.93	1.13	0.05	2.291	36.32	86.35	46.61	T
b6	1.07	1.14	0.05	2.360	34.57	88.85	47.27	T

^a $d_{C-H\cdots\pi}$ is the distance between H and the center of the phenyl ring. ^b ΔE_0 includes zero-point vibrational energy (ZPVE). ^cBW were calculated on the basis of the ΔE_0 with dispersion energy.

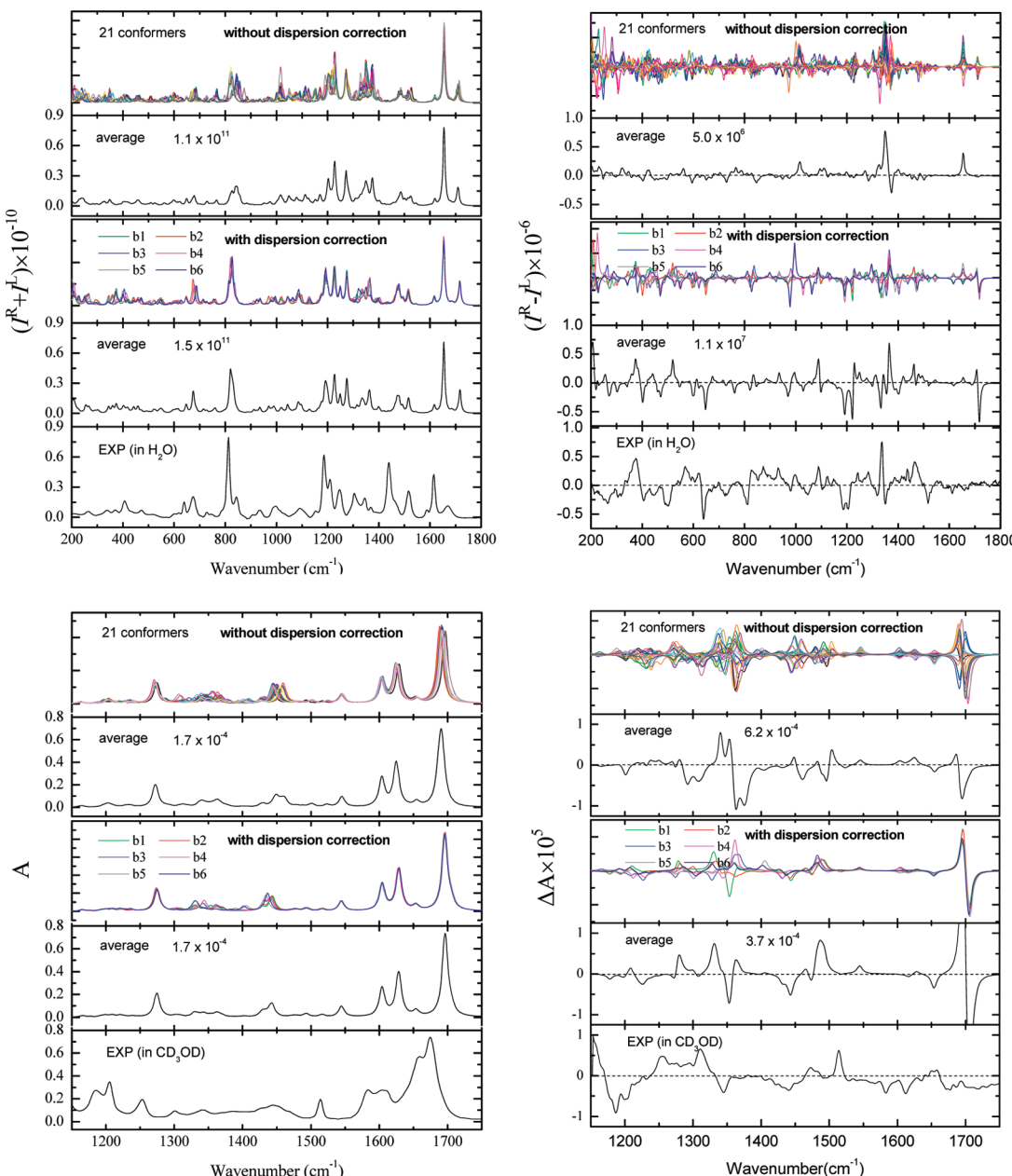


Figure 3. Calculated and experimental Raman ($I^R + I^L$), ROA ($I^R - I^L$), IR (A), and VCD (ΔA) spectra for the RS stereoisomer of protonated CATM. The calculated spectra were obtained using the B3LYP functional (with and without disp. correction) and 6-31++G***/IEFPCM level of theory. The average is based on the Boltzmann statistics in Table 1. Lorentzian band with the full width at half-maximum of 10 cm^{-1} was used. Calculated Raman and ROA intensities were multiplied by a factor to match experiment.

interaction. To some extent, the π -group acts as a hydrogen bond acceptor, while the C–H group acts as a hydrogen bond donor.⁸⁵ Relative energies, Boltzmann weights, and selected geometry parameters of these conformers are collected in Table 1, simulated Raman, ROA, IR, and VCD spectra are displayed in Figure 3. The pure B3LYP functional fails to reproduce the experimental ROA and VCD spectra. However, spectra obtained by B3LYP-D are in good agreement with experiment.

Geometry and Stability of DKP Diastereoisomers.

Optimized geometries of the most stable conformers as computed at the B3LYP-D/6-31++G**/IEFPCM(H₂O) level of theory are shown in Figure 2 (for RS) and Figure 4 (SS).

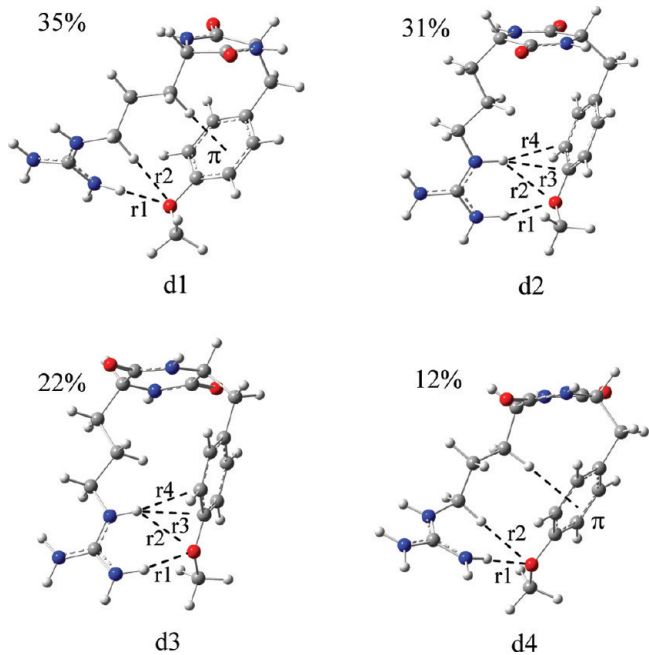


Figure 4. Four most stable SS conformers of protonated CATM, obtained at the B3LYP-D/6-31++G**/IEFPCM(H₂O) level of theory. Structures d1 and d4 differ by the opposite orientation between the protonated guanidine group and OMe positions, and they are stabilized by the N–H···O, C–H···O, and C–H··· π intramolecular interactions; d2 and d3 are mainly stabilized by N–H···O hydrogen bonds. The Boltzmann weights were calculated from their relative energies with ZPVE correction (see Table 2).

In RS (and its mirror image, SR, which is not shown), because of an intramolecular interaction between the aromatic ring of the tyrosine residue and the DKP ring, a folded conformation is favored over the other structures, which is consistent with an earlier conformational study of cyclic dipeptides.⁸⁶ There are

three pairs of conformers (b1 vs b2, b3 vs b4, and b5 vs b6) differing in the OMe position. As can be seen from Table 1, the relative stability of these conformers changes marginally upon inclusion of the zero-point vibrational energy (ZPVE). The energetic ordering is also almost unaffected by the OMe positions, e.g., the b1 and b2 structures have almost identical Boltzmann weights, 35% and 32%, respectively. For b3–6, the arginine side chain adopts an equatorial conformation with respect to the DKP ring. The folded structures are stabilized by C_α–H··· π (phenyl) intramolecular interactions, which leads to a rather short separation of the arginine and tyrosine side chains of 2.291–2.465 Å (see Table 1).

The SS molecule adopts only four stable conformations (Figure 4). From the relative conformer energies (Table 2), we see that unlike for RS, the energetic ordering is changed by the inclusion of ZPVE corrections. The orientation of the protonated arginine chain relative to the OMe groups also significantly influences the total electronic energy. For instance, d1 and d4 only differ in the relative orientation, but exhibit a large relative energy difference (0.62 kcal/mol), resulting in Boltzmann populations of 35% and 12%, respectively. The most stable SS(RR) conformer is the folded d1. For all stable structures of SS and RR, the arginine and tyrosine(OMe) side chains are located on the same side of the DKP ring. Structures d1 and d4 can be characterized by their N–H···O, C–H···O, and C–H··· π interactions; the d2 and d3 conformers are mainly stabilized by N–H···O hydrogen bonds in the protonated guanidine group.

Thus, the AC is intertwined with molecular conformational properties. The orientation of the side chain plays a crucial role especially in the stability of the SS and RR DKP derivatives. The hydrogen bonds and C–H··· π interactions are significant factors in determining the structures of these compounds.

Conformation of the Dipeptide Ring. The conformation may be viewed as boat (B), twist-boat (T), chair (C), half-chair (H), envelop (E), or screw-boat (S). Computed coordinate values for RS and SS are listed in Tables 1 and 2, respectively. It is seen from Table 1 that the θ values are close to 90°, with deviations up to 5.6°, while the P_2 values are almost 50° or $\pi + 50^\circ$, with deviations smaller than 3.4°. Thus, the most preferred conformation of the DKP ring in RS and SR is the twist-boat (T), down for RS and up for SR.

For SS/RR, the DKP rings have different conformations. The d1 and d4 structures adopt pure boat-down and twist-boat-down, respectively; the d2 and d3 structures are similar but with rather small puckering amplitudes (only 4.06° and 7.44°, respectively, see Table 2), i.e., d2 and d3 tend to be nearly planar (P). For RS and SR, the twist-boat (T) conformation is preferred, independent of the orientation of the tyrosine(OMe)

Table 2. Relative Energies (ΔE , kcal/mol), Boltzmann Weights (BW, 298.15 K), C_β–H··· π Distance^a ($d_{C-H\cdots\pi}$, Å), Intramolecular Hydrogen Bonds (r_{1-4} , Å, see Figure 4), and Pseudorotational Parameters (Q, θ , and P_2 , deg) of Stable SS Conformers with Dispersion Correction for Protonated CATM, Obtained at B3LYP-D/6-31++G/IEFPCM(H₂O) Level of Theory**

conformer	ΔE	ΔE_0^b	BW ^c	$d_{C-H\cdots\pi}$	r_1	r_2	r_3	r_4	pseudorotational parameters			
									Q	θ	P_2	shape
d1	0.00	0.00	0.35	2.314	1.889	2.422			17.97	87.88	33.51	B
d2	0.79	0.07	0.31		1.998	2.473	2.383	2.506	4.06	81.34	178.88	T → P
d3	0.69	0.26	0.22		2.037	2.478	2.395	2.521	7.44	89.12	90.89	B → P
d4	0.49	0.62	0.12	2.287	1.887	2.420			23.93	83.13	60.03	T

^a $d_{C-H\cdots\pi}$ is the distance between H and the center of the phenyl ring. ^b ΔE_0 includes zero-point vibrational energy (ZPVE). ^cBW were calculated on the basis of the ΔE_0 with dispersion energy.

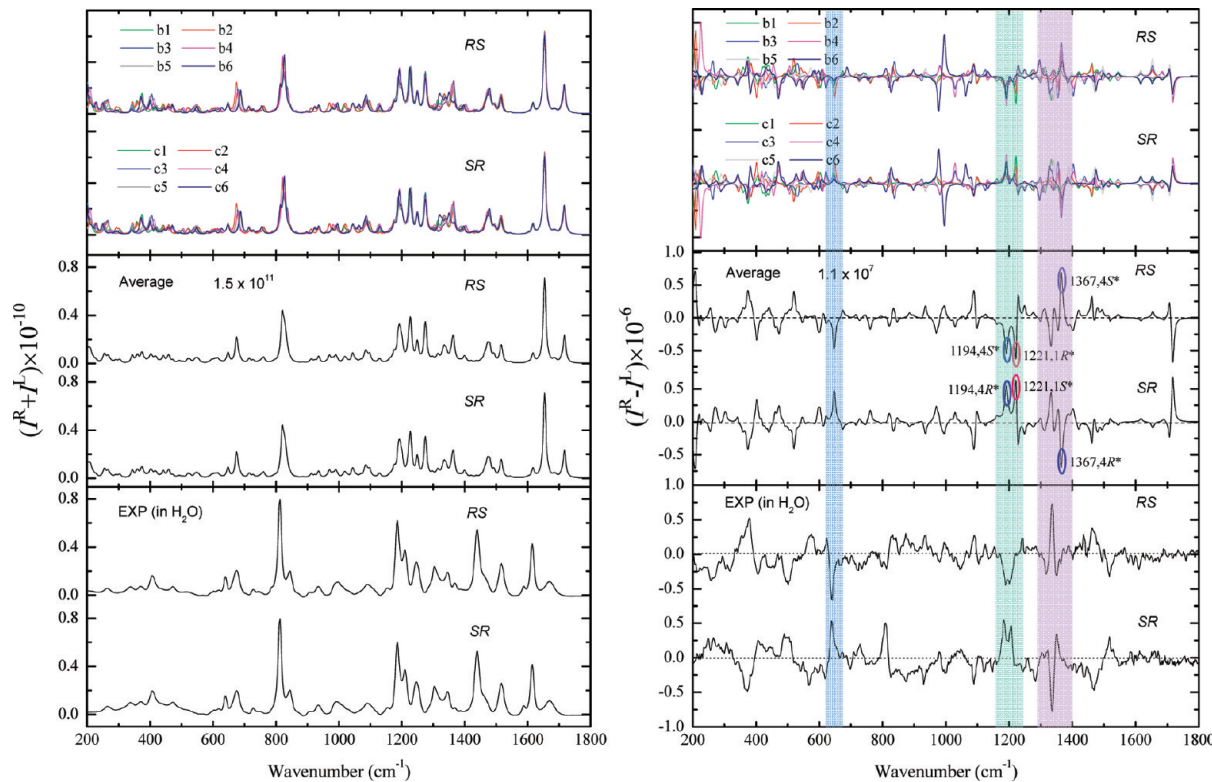


Figure 5. Calculated (B3LYP-D/6-31++G***/IEFPCM(H₂O), top and middle pannels) and experimental (in aqueous solution, bottom) Raman ($I^R + I^L$) and ROA ($I^R - I^L$) spectra of RS and SR protonated CATM stereoisomers. Average spectra were generated using Boltzmann statistics.

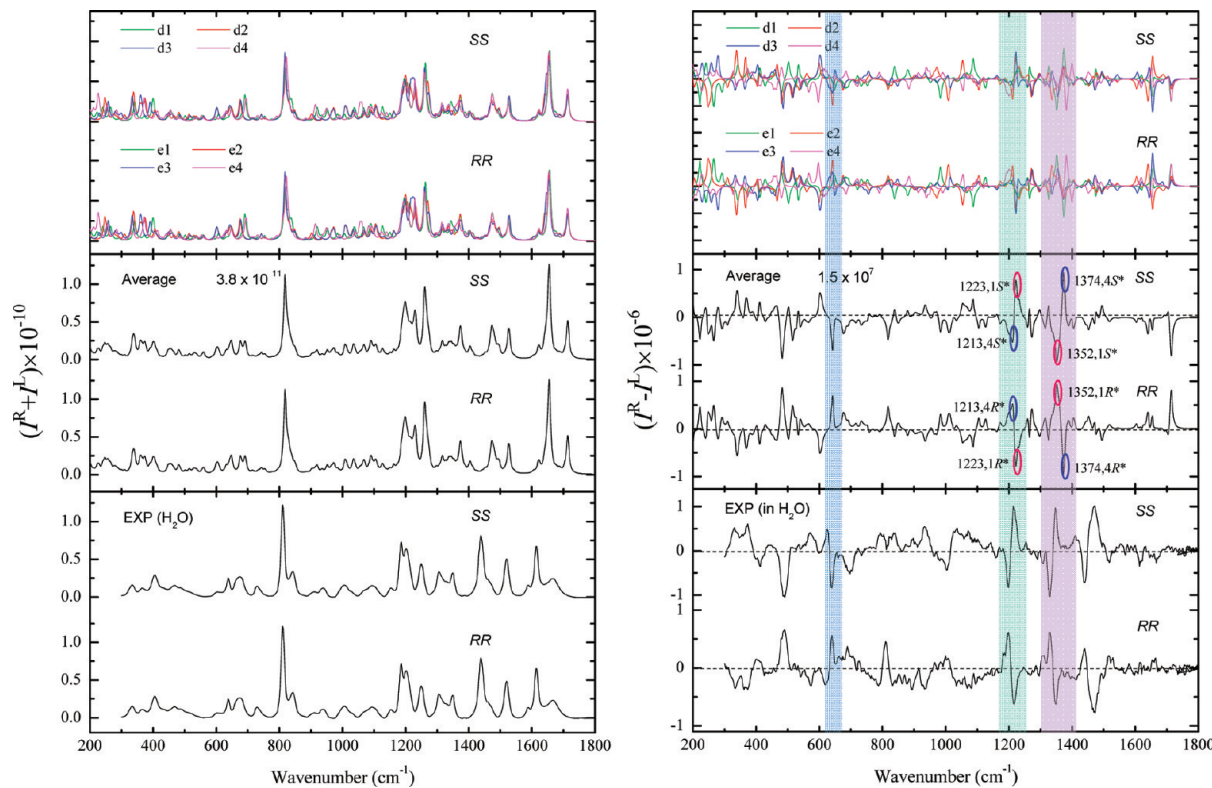


Figure 6. Calculated and experimental spectra of the SS and RR isomers; the layout is analogous to that in Figure 5.

and arginine side chains. For SS and RR, however, there is an obvious correlation between the DKP ring and the positions of the two side chains, which is due to the fact that the latter both are located on the same side of the DKP ring.

Vibrational Optical Activity Spectra. The calculated Raman and ROA spectra of the four stereoisomers (RS, SR, SS, and RR) of protonated CATM determined at the B3LYP-D/6-31++G***/IEFPCM(H₂O) level of theory are shown in

Table 3. Observed and Calculated Vibrational Wavenumbers (cm^{-1}) and Assignments of Most Distinct ROA Bands of Protonated CATM^a

observed		calculated		ROA patterns				assignment
RS/SR	SS/RR	RS/SR	SS/RR	RS	SR	SS	RR	
		1716s	1714s	—	+	—	+	$\nu \text{C}=\text{O}$ (amide I)
1550–1700								$\delta \text{NH}_2, \beta \text{C}-\text{H}, \nu \text{C}-\text{C}(\text{Phe})$
1517m	1468vs	1519vw	1493vw	—	+	+	—	$\delta \text{CH}_2, \alpha_s \text{CH}_3$
1465m	1442s	1462w	1451vw	+	—	—	+	ring $\beta \text{N}-\text{H}, \nu \text{C}-\text{N}$ (amide II), and $\nu \text{C}-\text{C}(\text{Phe})$
1351m	1366vw	1387w	1388w	—	+	—	+	ring $\beta \text{N}-\text{H}, \alpha \text{C}_\alpha-\text{H}, \text{t CH}_2$
1336vs	1347vs	1365vs	1373vs	+	—	+	—	$\alpha \text{C}_\alpha-\text{H}, \omega \text{C}_\beta\text{H}_2, \beta \text{C}-\text{H}(\text{Phe})$
	1330vs		1352vs			—	+	$\alpha \text{C}_\alpha-\text{H}, \text{t CH}_2, \text{ring } \beta \text{N}-\text{H}$
1319m		1331w		—	+			$\alpha \text{C}_\alpha-\text{H}, \text{t CH}_2, \text{ring } \beta \text{N}-\text{H}$
1204vs	1215vs	1221vs	1223vs	—	+	+	—	$\text{t C}_\beta\text{H}_2, \alpha \text{C}_\alpha-\text{H}$
1186vs	1200vs	1194vs	1213vs	—	+	—	+	$\text{t C}_\beta\text{H}_2, \nu \text{C}_\alpha-\text{C}_\beta, \alpha \text{C}_\alpha-\text{H}$
1088m	1033m	1088s	1052m	+	—	+	—	$\nu \text{C}-\text{N}, \text{t CH}_2$
1047w	1003w	1028vw	1011m	—	+	—	+	$\text{t CH}_2, \rho \text{CH}_2, \alpha \text{C}_\alpha-\text{H}$
998w		994w		+	—			$\nu \text{C}-\text{C}, \nu \text{C}-\text{N}, \rho \text{NH}_2$
980vw		970w		—	+			$\nu \text{C}-\text{C}, \nu \text{C}-\text{N}, \rho \text{NH}_2$
931m	936m	934w	936w	+	—	+	—	$\nu \text{C}_\alpha-\text{C}_\beta, \rho \text{CH}_2, \gamma_{as} \text{C}-\text{H}(\text{Phe})$
325w	333w	333vw	337vw	+	—	+	—	$\gamma \text{C}-\text{H}(\text{Phe}), \rho \text{CH}_2, \alpha \text{N}-\text{C}-\text{C}_\alpha$
810m/s	813w/s	819vw	817m	—	+	—	+	Phe breathing, $\alpha \text{N}-\text{C}-\text{C}_\alpha$
728w	694w	758vw	678w	—	+	—	+	$\nu \text{C}-\text{C}, \alpha \text{C}-\text{C}-\text{C}, \gamma_s \text{C}-\text{H}(\text{Phe})$
640s	639m	646m	642m	—	+	—	+	ring $\gamma \text{N}-\text{H}, \beta \text{C}-\text{C}-\text{C}(\text{Phe})$
621w	624m	623vw	626m	+	—	+	—	ring $\gamma \text{N}-\text{H}, \rho \text{NH}_2$
568m	573w	519s	502vw	+	—	+	—	ring $\gamma \text{N}-\text{H}$
497m	489vs	472m	481s	—	+	—	+	ring $\gamma \text{N}-\text{H}$
406w	412w	401m	403vw	—	+	—	+	skeletal breathing, $\beta \text{C}=\text{O}, \gamma \text{N}-\text{H}$
376s	373s	373m	368m	+	—	+	—	$\rho \text{CH}_2, \gamma \text{C}(\text{Phe})-\text{O}$
			338m			+	—	$\tau \text{CH}_3, \gamma \text{C}(\text{Phe})-\text{O}, \text{ring } \rho \text{N}-\text{H}$

^aAbbreviations: ν , stretching; ω , wagging; δ , scissoring; τ , twisting; ρ , rocking; α , bending; α_s , symmetric bending; β , in-plane bending; γ , out-of-plane bending; τ , torsion. Relative intensity: very weak (vw), weak (w), medium (m), strong (s).

Figures 5 and 6, respectively, together with the experimental spectra. The averaged theoretical spectra were generated from the Boltzmann weights listed in Tables 1 and 2. For each stereoisomer, the calculated ROA subspectra of the most stable conformers show a strong conformational dependence. The flexibility of the side chains affects the spectral bands significantly, except for the orientations of the methoxy group.

The calculated ROA spectra are in good agreement with experiment. Vibrational wavenumbers and assignments for the most distinct ROA peaks are summarized in Table 3. The computed ROA bands at 642 and 646 cm^{-1} (experimentally at 639 and 640 cm^{-1}) are assigned to the N–H out-of-plane bending in the dipeptide DKP ring, and C–C–C deformation of the phenyl ring. The signal at 1186–1223 cm^{-1} mainly originates from the two chiral centers (the C_1 and C_4 atoms, Figure 1), and the positive (+) or negative (−) ROA can be used to determine the R or S chirality. For example, in the average ROA spectrum, the peak at 1194 (or 1213) cm^{-1} is characteristic of 4R (+) and 4S (−) forms, whereas the peak at 1221 (or 1223) cm^{-1} is characteristic of the 1R (−) and 1S (+) forms. For the RS isomer, therefore, there are two negative peaks, in which the first negative peak is mainly dominated by $\text{C}_\alpha-\text{C}_\beta$ stretching and $\text{C}_\alpha-\text{H}$ bending of the 4S part, combined with its strong CH_2 twisting vibration; and the second negative peak arises from the involvement of strong CH_2 twisting and $\text{C}_\alpha-\text{H}$ bending vibrations of the 1R part. Similarly, in the 1319–1373 cm^{-1} region, there are also some characteristic peaks that can be used to identify the R or S form; especially for SS and RR, there are two opposite couples, (−+) for SS and (+−)

for RR, with the contributions from $\text{C}_\alpha-\text{H}$ bending, N–H in-plane bending, and CH_2 twisting vibrations of 1S or 1R and $\text{C}_\alpha-\text{H}$ bending and C_βH_2 wagging of 4S or 4R.

A shoulder at 1716 (or 1714) cm^{-1} is characteristic of the amide I band, which arises from the carbonyl $\text{C}=\text{O}$ stretching. Because of the band broadening originating from hydrogen bonding (which is only described implicitly by the employed solvent model), the calculated intensity is much larger than in the experiment. The amide II band is found in the 1442–1465 cm^{-1} region; its relative intensity is experimentally strong, but rather underestimated theoretically. The ROA sign patterns in the 1186–1223 and 1319–1373 cm^{-1} regions are therefore more important for determining the AC than the amide bands.

For comparison with IR and VCD experiments, we use spectra calculated in aqueous solution, as for ROA. This saves computational time since the two polar solvent environments (water and methanol) modeled with IEFPCM provide nearly the same conformer populations and vibrational properties (Supporting Information, Table S2 and Figure S3). As can be seen from Figures 7 and 8, the calculated VCD spectra reproduce most of the experimentally observed peaks. The averaged spectrum is dominated by the two most populated conformers (e.g., b1 and b2, etc.) because of their large Boltzmann weights (35% and 32% for b1 and b2, respectively).

As for ROA, several VCD bands can serve as fingerprints for the C_1 and C_4 chiral centers. They include a shoulder at ~1277 (or 1270) cm^{-1} (+ for 1R, − for 1S), a sharp peak at ~1345 (or 1360) cm^{-1} (− for 1R, + for 1S), and a weak peak at ~1368 cm^{-1} (− for 4R, + for 4S). For RS and SR; however, an

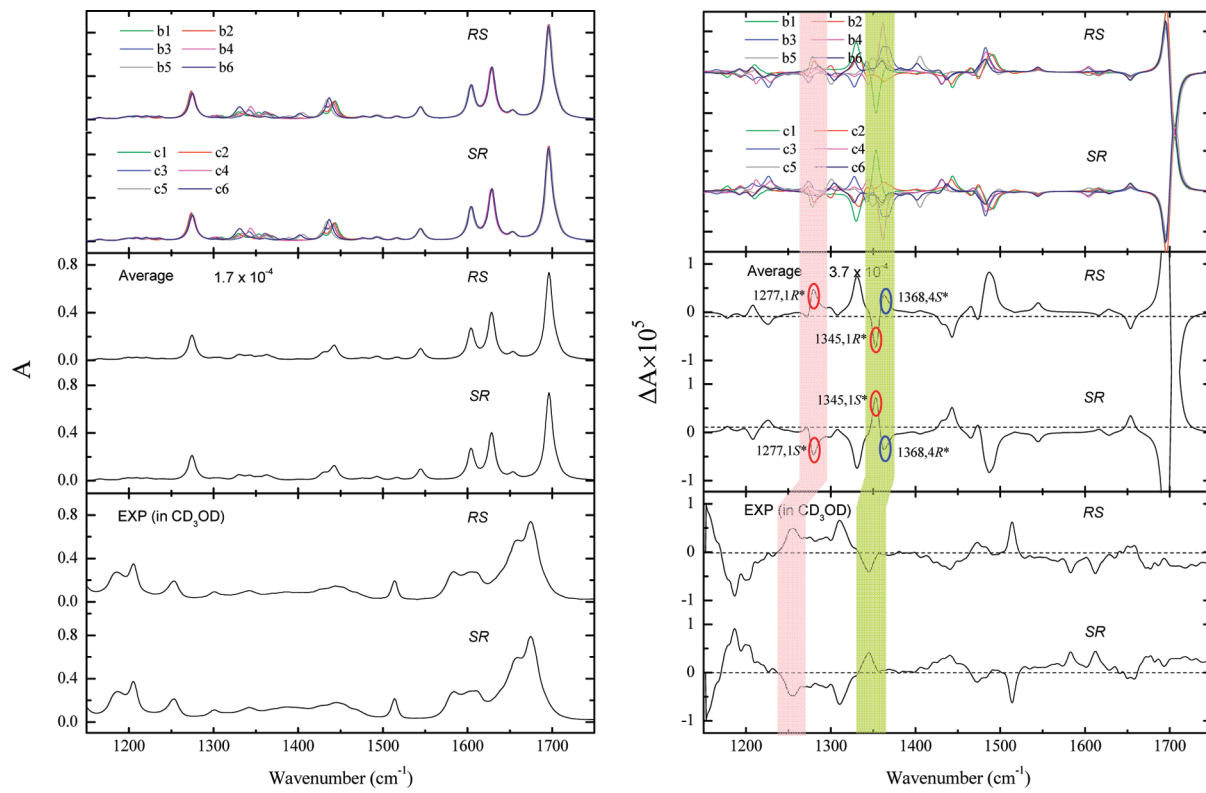


Figure 7. Calculated and experimental (in CD_3OD , bottom) IR and VCD spectra of RS and SR protonated CATM.

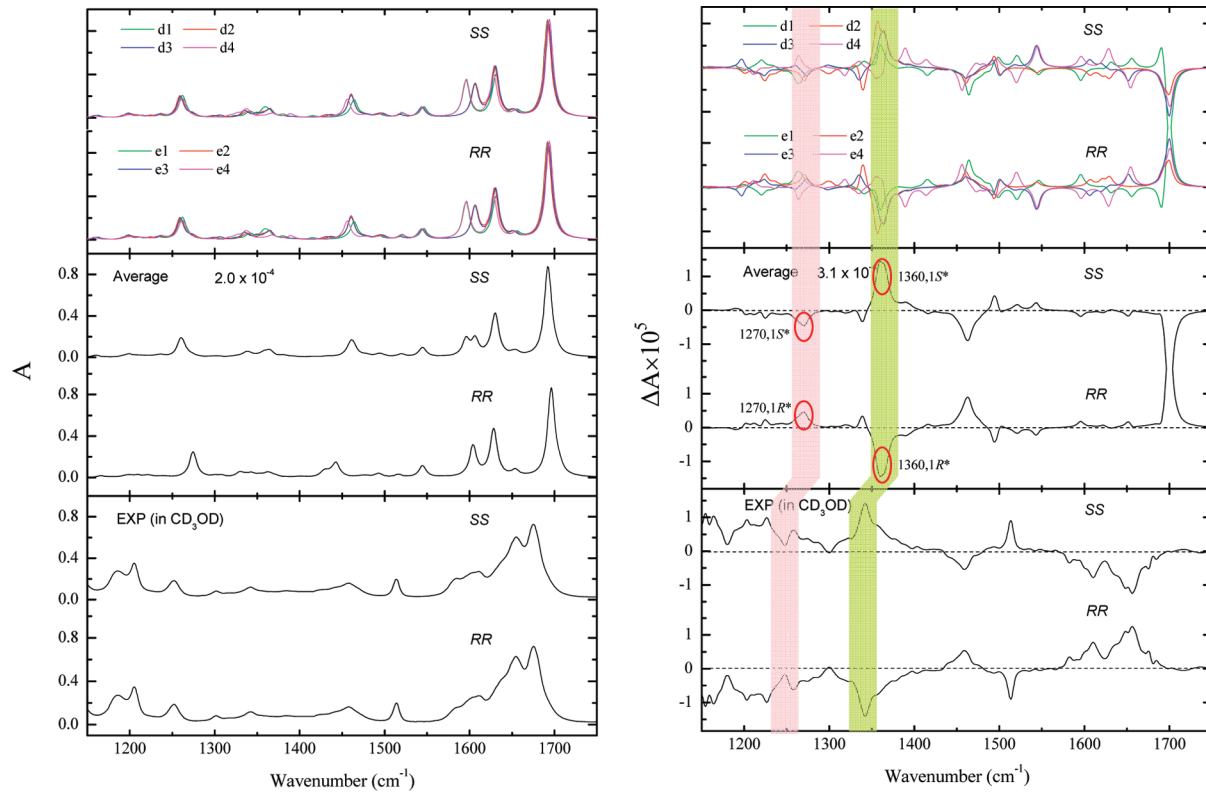


Figure 8. Calculated and experimental IR and VCD spectra of the SS and RR stereoisomers (see also Figure 7).

experimental VCD peak at $\sim 1368 \text{ cm}^{-1}$ is not observed, due to the overlap with the solvent (CD_3OD) signal. In the calculated SS or RR spectra, there is a broad peak located around 1360 cm^{-1} because the 1S (+, $\sim 1345 \text{ cm}^{-1}$) and

4S (+, $\sim 1368 \text{ cm}^{-1}$) or 1R (-, $\sim 1345 \text{ cm}^{-1}$) and 4R (-, $\sim 1368 \text{ cm}^{-1}$) signals overlap.

Taking the RS isomer as an example, the weak positive band located at 1277 cm^{-1} is assigned to $\text{C}_\alpha\text{-H}$ bending and CH_2

wagging vibrations of the 1R part; the sharp negative peak at 1345 cm^{-1} has contributions from $\text{C}_\alpha\text{--H}$ bending and CH_2 twisting vibrations of 1R; and the weak positive peak at 1368 cm^{-1} is dominated mainly by $\text{C}_\alpha\text{--H}$ bending and C_βH_2 wagging of the 4S part; in addition, in the $1442\text{--}1493\text{ cm}^{-1}$ region, strong CH_2 scissoring of 1R (or 4S) and N–H in-plane bending vibrations dominate the VCD bands, and they should therefore not be viewed as characteristic peaks to identify the two chiral forms. We note that all the calculated VCD bands have somewhat larger frequencies in comparison to the experimental spectra because of the anharmonic effects and explicit hydrogen bonding interactions not included in the IEPCM model.

Nevertheless, the present study demonstrates that both ROA and VCD can be used to determine the absolute configuration of conformationally flexible molecules with two chiral centers. Obviously, as the precision of the simulation and experiment increases, AC resolutions of more than two chiral center systems should be possible in the future. To ameliorate the reliability of the mixed experimental/theoretical approach for structure determination of chiral molecules, one needs to consider many aspects. In the case of CATM, in particular, the conformer equilibrium had to be properly treated. Of the two vibrational chiroptical spectroscopies, ROA is perhaps more useful for our molecule than VCD, as it comprises a larger wavenumber region and is more sensitive to the configuration at both stereogenic centers.

CONCLUSIONS

We have investigated the ability of a combined theoretical and experimental approach to vibrational chiroptical spectroscopy (ROA and VCD) to determine the absolute configuration of conformationally flexible molecules with two chiral centers, using the cyclic dipeptide CATM as a test case. Both the experimental and the theoretical spectra for all stereoisomers of CATM were reported. The B3LYP-D dispersion-corrected approach was imperative for accurate modeling of the conformer equilibria. The resulting calculated spectra were in good agreement with the experimental data. Thus, the ROA and VCD techniques are able to resolve the absolute configuration of flexible molecules with two chiral centers. The orientation of the side chains played a key role in the stability of the conformations, in particular, for the SS and RR stereoisomers. Both the polar hydrogen bonding and the nonpolar C–H $\cdots\pi$ and dispersion interactions are significant factors for the stability and structure of the conformers. The RS and SR isomers adopt the twist-boat (T) DKP conformation with the twist-boat-down for RS and twist-boat-up for SR, relatively independently of the orientation of the arginine and tyrosine-(OMe) side chains. For SS and RR, however, there is a strong correlation between the DKP ring geometry and the two side-chain geometries. The ROA sign patterns in the regions $1186\text{--}1223$ and $1319\text{--}1373\text{ cm}^{-1}$ are the most important characteristic of the CATM stereoisomers.

ASSOCIATED CONTENT

Supporting Information

Computed relative energies for RS protonated CATM employing the DFT method without dispersion correction and additional computational results. This material is available free of charge via the Internet at <http://pubs.acs.org>.

AUTHOR INFORMATION

Corresponding Author

*E-mail: kenneth.ruud@uit.no (K.R.); bour@uochb.cas.cz (P.B.).

Notes

The authors declare no competing financial interest.

ACKNOWLEDGMENTS

This work was supported by the Research Council of Norway through a Centre of Excellence grant (Grant No. 179568) and a research grant (Grant No. 191251). P.B. was supported by Academy of Sciences (M200550902), Grant Agency of the Czech Republic (P208/11/0105), and Ministry of Education (LH11033). A grant of computer time from the Norwegian supercomputing program NOTUR is gratefully acknowledged.

REFERENCES

- (1) Martins, M. B.; Carvalho, I. *Tetrahedron* **2007**, *63*, 9923–9932.
- (2) Ginz, M.; Engelhardt, U. H. *J. Agric. Food Chem.* **2000**, *48*, 3528–3532.
- (3) Fischer, P. M. *J. Peptide Sci.* **2003**, *9*, 9–35.
- (4) Kawamura, K.; Takeya, H.; Kushibe, T. *Adv. Space Res.* **2009**, *44*, 267–275.
- (5) Atkin, C. L.; Neilands, J. B. *Biochemistry* **1968**, *7*, 3734–3739.
- (6) Bodanszky, M.; Sigler, G. F.; Bodanszky, A. *J. Am. Chem. Soc.* **1973**, *95*, 2352–2357.
- (7) Lucietto, F. R.; Milne, P. J.; Kilian, G.; Frost, C. L.; Venter, M. V. D. *Peptides* **2006**, *27*, 2706–2714.
- (8) Kilian, G.; Jamie, H.; Brauns, S. C. A.; Dyason, K.; Milne, P. J. *Pharmazie* **2005**, *60*, 305–309.
- (9) Imamura, M.; Prasad, C. *Peptides* **2003**, *24*, 445–448.
- (10) López-Rodríguez, M. L.; Morcillo, M. J.; Fernández, E.; Porras, E.; Orensan, L.; Beneytez, M. E.; Manzanares, J.; Fuentes, A. J. A. *J. Med. Chem.* **2001**, *44*, 186–197.
- (11) Wyatta, P. G.; Allenb, M. J.; Borthwicka, A. D.; Daviesa, D. E.; Exalla, A. M.; Hatleya, R. J. D.; Irvinga, W. R.; Livermorea, D. G.; Millera, N. D.; Nerozzia, F.; Sollisa, S. L.; Szardenings, A. K. *Bioorg. Med. Chem. Lett.* **2005**, *15*, 2579–2582.
- (12) Brauns, S. C.; Milne, P.; Naudé, R.; Venter, M. V. D. *Anticancer Res.* **2004**, *24*, 1713–1720.
- (13) Trischman, J. A.; Oeffner, R. E.; Luna, M. G. D.; Kazaoka, M. *Mar. Biotechnol.* **2004**, *6*, 215–220.
- (14) Fukushima, K.; Yazawa, K.; Arai, T. *J. Antibiot.* **1973**, *26*, 175–176.
- (15) Sinha, S.; Srivastava, R.; Clercq, E. D.; Singh, R. K. *Nucleosides, Nucleotides Nucleic Acids* **2004**, *23*, 1815–1824.
- (16) Bettens, F. L.; Bettens, R. P. A.; Brown, R. D.; Godfrey, P. D. *J. Am. Chem. Soc.* **2000**, *122*, 5856–5860.
- (17) Brady, G. P.; Sharp, K. A. *Biophys. J.* **1997**, *72*, 913–927.
- (18) Brienne, M.-J.; Gabard, J.; Leclercq, M.; Lehn, J.-M.; Cesario, M.; Pascard, C.; Chev  , M.; Dutruc-Rosset, G. *Tetrahedron Lett.* **1994**, *35*, 8157–8160.
- (19) Blancoa, F.; Alkorta, I.; Rozas, I.; Elguero, J. *J. Phys. Org. Chem.* **2010**, *23*, 1155–1172.
- (20) McCleland, K.; Milne, P. J.; Lucieto, F. R.; Frost, C.; Brauns, S. C.; Venter, M. V. D.; Plessis, J. D.; Dyason, K. *J. Pharm. Pharmacol.* **2004**, *56*, 1143–1153.
- (21) Civalleri, B.; Zicovich-Wilson, C. M.; Valenzano, L.; Ugliengo, P. *CrystEngComm* **2008**, *10*, 405–410.
- (22) Dabkowska, I.; Gonzalez, H. V.; Jure  ka, P.; Hobza, P. *J. Phys. Chem. A* **2005**, *109*, 1131–1136.
- (23) Johnson, E. R.; Wolkow, R. A.; DiLabio, G. A. *Chem. Phys. Lett.* **2004**, *394*, 334–338.
- (24) Grimme, S. *J. Comput. Chem.* **2004**, *25*, 1463–1473.
- (25) Grimme, S. *J. Comput. Chem.* **2006**, *27*, 1787–1799.
- (26) Parac, M.; Etinski, M.; Peric, M.; Grimme, S. *J. Chem. Theory Comput.* **2005**, *1*, 1110–1118.

- (27) Piacenza, M.; Grimme, S. *J. Am. Chem. Soc.* **2005**, *127*, 14841–14848.
- (28) Feng, C.; Lin, C. S.; Fan, W.; Zhang, R. Q.; Hove, M. A. V. *J. Chem. Phys.* **2009**, *131*, 194702–8.
- (29) Kim, D.; Brédas, J.-L. *J. Am. Chem. Soc.* **2009**, *131*, 11371–11380.
- (30) Barron, L. D. *Molecular Light Scattering and Optical Activity*, 2nd ed.; Cambridge University Press: Cambridge, U.K., 2004.
- (31) Ruud, K.; Helgaker, T.; Bouř, P. *J. Phys. Chem. A* **2002**, *106*, 7448–7455.
- (32) Hug, W.; Kint, S.; Bailey, G. F.; Scherer, J. R. *J. Am. Chem. Soc.* **1975**, *97*, 5589–5590.
- (33) Pecul, M.; Ruud, K. *Int. J. Quantum Chem.* **2005**, *104*, 816–829.
- (34) Ruud, K.; Thorvaldsen, A. J. *Chirality* **2009**, *21*, E54–E67.
- (35) Stephens, P. J. *J. Phys. Chem. A* **1985**, *89*, 748–752.
- (36) Nafie, L. A.; Cheng, J. C.; Stephens, P. J. *J. Am. Chem. Soc.* **1975**, *97*, 3842–3843.
- (37) Hopmann, K. H.; Ruud, K.; Pecul, M.; Kudelski, A.; Dračinský, M.; Bouř, P. *J. Phys. Chem. B* **2011**, *115*, 4128–4137.
- (38) Pecul, M.; Lamparska, E.; Cappelli, C.; Frediani, L.; Ruud, K. *J. Phys. Chem. A* **2006**, *110*, 2807–2815.
- (39) Gómez-Hurtado, M. A.; Torres-Valencia, J. M.; Manríquez-Torres, J.; Río, R. E. D.; Motilva, V.; García-Maurino, S.; Ávila, J.; Talero, E.; Cerdá-García-Rojas, C. M.; Joseph-Nathan, P. *Phytochemistry* **2011**, *72*, 409–414.
- (40) Mukhopadhyay, P.; Zuber, G.; Beratan, D. N. *Biophys. J.* **2008**, *95*, 5574–5586.
- (41) Keiderling, T. A.; Silva, R. A. G. D.; Yoder, G.; Dukor, R. K. *Bioorg. Med. Chem.* **1999**, *7*, 133–141.
- (42) Kapitán, J.; Baumruk, V.; Bouř, P. *J. Am. Chem. Soc.* **2006**, *128*, 2438–2443.
- (43) Abdali, S.; Jalkanen, K. J.; Cao, X.; Nafie, L. A.; Bohr, H. *Phys. Chem. Chem. Phys.* **2004**, *6*, 2434–2439.
- (44) McColl, I. H.; Blanch, E. W.; Hecht, L.; Barron, L. D. *J. Am. Chem. Soc.* **2004**, *126*, 8181–8188.
- (45) Polyanichko, A.; Wieser, H. *Spectroscopy* **2010**, *24*, 239–244.
- (46) Blanch, E. W.; Hecht, L.; Syme, C. D.; Volpetti, V.; Lomonosoff, G. P.; Barron, L. D. *J. Gen. Virol.* **2002**, *83*, 2593–2600.
- (47) Qiu, F.; Zhang, Y.; Caceres-Cortes, J.; Reily, M. D. *Am. Lab.* **2010**, *42*, 33–34.
- (48) Nieto-Ortega, B.; Casado, J.; Blanch, E. W.; Navarrete, J. T. L.; Quesada, A. R.; Ramirez, F. J. *J. Phys. Chem. A* **2011**, *115*, 2752–2755.
- (49) Zuber, G.; Hug, W. *Helv. Chim. Acta* **2004**, *87*, 2208–2234.
- (50) Stephens, P. J.; McCann, D. M.; Devlin, F. J.; A. B. Smith, I. *J. Nat. Prod.* **2006**, *69*, 1055–1064.
- (51) Stephens, P. J.; Pan, J. J.; Devlin, F. J.; Krohn, K.; Kurtán, A. T. *J. Org. Chem.* **2007**, *72*, 3521–3536.
- (52) Polavarapu, P. L.; Donahue, E. A.; Shanmugam, G.; Scalmani, G.; Hawkins, E. K.; Rizzo, C.; Ibnusaud, I.; Thomas, G.; Habel, D.; Sebastian, A. D. *J. Phys. Chem. A* **2011**, *115*, 5665–5673.
- (53) Celik, S.; Ozel, A. E.; Akyuz, S.; Kecel, S.; Agaeva, G. *J. Mol. Struct.* **2011**, *993*, 341–348.
- (54) Mendham, A. P.; Palmer, R. A.; Potter, B. S.; Dines, T. J.; Snowden, M. J.; Withnall, R.; Chowdhry, B. Z. *J. Raman Spectrosc.* **2010**, *41*, 288–302.
- (55) Mendham, A. P.; Dines, T. J.; Snowden, M. J.; Withnall, R.; Chowdhry, B. Z. *J. Raman Spectrosc.* **2009**, *40*, 1508–1520.
- (56) Mendham, A. P.; Potter, B. S.; Palmer, R. A.; Dines, T. J.; Mitchell, J. C.; Withnall, R.; Chowdhry, B. Z. *J. Raman Spectrosc.* **2010**, *41*, 148–159.
- (57) Mendham, A. P.; Dines, T. J.; Withnall, R.; Mitchell, J. C.; Chowdhry, B. Z. *J. Raman Spectrosc.* **2009**, *40*, 1498–1507.
- (58) Mendham, A. P.; Dines, T. J.; Snowden, M. J.; Chowdhry, B. Z.; Withnall, R. *J. Raman Spectrosc.* **2009**, *40*, 1478–1497.
- (59) Bouř, P.; Sychrovský, V.; Maloň, P.; Hanzlíková, J.; Baumruk, V.; Pospíšek, J.; Buděšínský, M. *J. Phys. Chem. A* **2002**, *106*, 7321–7327.
- (60) Kopple, K. D.; Ohnishi, M. *J. Am. Chem. Soc.* **1969**, *91*, 962–970.
- (61) Davies, D. B.; Khaled, M. A. *J. Chem. Soc., Perkin Trans. 1* **1976**, *2*, 1238–1244.
- (62) Fava, G. G.; Belicchi, M. F.; Marchelli, R.; Dossena, A. *Acta Crystallogr.* **1981**, *B37*, 625–629.
- (63) Bowman, R. L.; Kellerman, M.; Johnson, W. C. *J. Biopolymers* **1983**, *22*, 1045–1070.
- (64) Tamburro, A. M.; Guantieri, V.; Scatturin, A. *Int. J. Biol. Macromol.* **1982**, *4*, 126–127.
- (65) Li, Z.; Mukamel, S. *J. Phys. Chem. A* **2007**, *111*, 11579–11583.
- (66) Wiedemann, S.; Metsala, A.; Nolting, D.; Weinkauf, R. *Phys. Chem. Chem. Phys.* **2004**, *6*, 2641–2649.
- (67) Ajo, D.; Granozzi, G.; Guantieri, V.; Tamburro, T. A. *J. Mol. Struct.* **1983**, *96*, 369–372.
- (68) Prasad, C. *Peptides* **1995**, *16*, 151–164.
- (69) Houston, D. R.; Synstad, B.; Eijsink, V. G. H.; Stark, M. J. R.; Eggleston, I. M.; Aalten, D. M. F. V. *J. Med. Chem.* **2004**, *47*, 5713–5720.
- (70) Houston, D. R.; Eggleston, I.; Synstad, B.; Eijsink, V. G. H.; Aalten, D. M. F. V. *Biochem. J.* **2002**, *368*, 23–27.
- (71) Hopmann, K. H.; Šebestík, J.; Novotná, J.; Stensen, W.; Urbanová, M.; Svenson, J.; Svendsen, J. S.; Bouř, P.; Ruud, K. *J. Org. Chem.* **2012**, *77*, 858–869.
- (72) Hug, W.; Hangartner, G. *J. Raman Spectrosc.* **1999**, *30*, 841–852.
- (73) Bouř, P.; Maloň, P. *The MCM Program*; Academy of Sciences: Prague, Czech Republic, 1995–2009.
- (74) Haasnoot, C. *J. Am. Chem. Soc.* **1992**, *114*, 882–887.
- (75) Cremer, D.; Pople, J. A. *J. Am. Chem. Soc.* **1975**, *97*, 1354–1358.
- (76) Becke, A. D. *Phys. Rev. A* **1988**, *38*, 3098–3100.
- (77) Lee, C.; Yang, W.; Parr, R. G. *Phys. Rev. B* **1988**, *37*, 785–789.
- (78) Frisch, M. J.; Trucks, G. W.; Schlegel, H. B.; Scuseria, G. E.; Robb, M. A.; Cheeseman, J. R.; Scalmani, G.; Barone, V.; Mennucci, B.; Petersson, G. A.; Nakatsuji, H.; Caricato, M.; Li, X.; Hratchian, H. P.; Izmaylov, A. F.; Bloino, J.; Zheng, G.; Sonnenberg, J. L.; Hada, M.; Ehara, M.; Toyota, K.; Fukuda, R.; Hasegawa, J.; Ishida, M.; Nakajima, T.; Honda, Y.; Kitao, O.; Nakai, H.; Vreven, T.; Montgomery, J. A., Jr.; Peralta, J. E.; Ogliaro, F.; Bearpark, M.; Heyd, J. J.; Brothers, E.; Kudin, K. N.; Staroverov, V. N.; Kobayashi, R.; Normand, J.; Raghavachari, K.; Rendell, A.; Burant, J. C.; Iyengar, S. S.; Tomasi, J.; Cossi, M.; Rega, N.; Millam, J. M.; Klene, M.; Knox, J. E.; Cross, J. B.; Bakken, V.; Adamo, C.; Jaramillo, J.; Gomperts, R.; Stratmann, R. E.; Yazyev, O.; Austin, A. J.; Cammi, R.; Pomelli, C.; Ochterski, J. W.; Martin, R. L.; Morokuma, K.; Zakrzewski, V. G.; Voth, G. A.; Salvador, P.; Dannenberg, J. J.; Dapprich, S.; Daniels, A. D.; Farkas, O.; Foresman, J. B.; Ortiz, J. V.; Cioslowski, J.; Fox, D. J. *Gaussian 09*, revision B.01; Gaussian, Inc.: Wallingford, CT, 2009.
- (79) Cancès, E.; Mennucci, B.; Tomasi, J. *J. Chem. Phys.* **1997**, *107*, 3032–10.
- (80) Tomasi, J.; Persico, M. *Chem. Rev.* **1994**, *94*, 2027–2094.
- (81) Tomasi, J.; Mennucci, B.; Cammi, R. *Chem. Rev.* **2005**, *105*, 2999–3094.
- (82) Biot, C.; Buisine, E.; Rooman, M. *J. Am. Chem. Soc.* **2003**, *125*, 13988–13994.
- (83) Yamamoto, S.; Straka, M.; Watarai, H.; Bouř, P. *Phys. Chem. Chem. Phys.* **2010**, *12*, 11021–11032.
- (84) Buděšínský, M.; Daněček, P.; Bednárová, L.; Kapitán, J.; Baumruk, V.; Bouř, P. *J. Phys. Chem. A* **2008**, *112*, 8633–8640.
- (85) Nishio, M. *CrystEngComm* **2004**, *6*, 130–158.
- (86) Kopple, K. D.; Marr, D. H. *J. Am. Chem. Soc.* **1967**, *89*, 6193–6200.